J. Fluid Mech. (2026), *vol.* 1030, A16, doi:10.1017/jfm.2026.11232

Bouncing to coalescence transition for droplet impact onto moving liquid pools

Daniel M. Harris[1], Luke Alventosa[1], Oliver Sand[1], Eli Silver[1], Arman Mohammadi[1], Thomas C. Sykes[2,3], Alfonso A. Castrejón-Pita[3] and Radu Cimpeanu[4]

[1]School of Engineering, Brown University, Providence, RI 02912, USA
[2]School of Engineering, University of Warwick, Coventry CV4 7AL, UK
[3]Department of Engineering Science, University of Oxford, Oxford OX1 3PJ, UK
[4]Mathematics Institute, University of Warwick, Coventry CV4 7AL, UK
Corresponding author: Daniel M. Harris, daniel_harris3@brown.edu

(Received 2 October 2025; revised 21 January 2026; accepted 25 January 2026)

A droplet impacting a deep fluid bath is as common as rain over the ocean. If the impact is sufficiently gentle, the mediating air layer remains intact, and the droplet may rebound completely from the interface. In this work, we experimentally investigate the role of translational bath motion on the bouncing to coalescence transition. Over a range of parameters, we find that the relative bath motion systematically decreases the normal Weber number required to transition from bouncing to merging. Direct numerical simulations demonstrate that the depression created during impact combined with the translational motion of the bath enhances the air-layer drainage on the upstream side of the droplet, ultimately favouring coalescence. A simple geometric argument is presented that rationalises the collapse of the experimental threshold data, extending what is known for the case of axisymmetric normal impacts to the more general three-dimensional scenario of interest herein.

Key words: drops, capillary flows, gas/liquid flow

1. Introduction

When two volumes of fluid approach one another in a gas, whether they be droplets, jets or a droplet and a bath, the outcome of the impact is determined by the properties and persistence of a thin interstitial gas layer (Rein 1993; Neitzel & Dell'Aversana 2002; Yarin 2006; Sprittles 2024). For relatively low-energy collisions in air, the liquids may rebound completely from one another having never made direct contact, provided the inertia of the liquid is insufficient to drain the air layer during the interaction. The critical role of the air layer was first hypothesised by Lord Rayleigh for the case of colliding jets, similarly framing the essential question as to '. . .whether the air can be anywhere squeezed out during the short time over which the collision extends' (Rayleigh 1899). More specifically, the air layer must drain to a sufficient thickness such that van der Waals forces can initiate coalescence, a length scale typically of the order of 0.1 μm (Couder *et al.* 2005; Tang *et al.* 2019; Sprittles 2024).

In the present work, we focus on the bouncing to coalescence (BC) transition for the case of a droplet impacting a deep planar bath, first examined in the seminal contribution of Schotland (1960). Schotland identified the transition between rebound and coalescence for a continuous stream of droplets impacting a fluid bath at an oblique angle. They noted that for a fixed liquid and gas pair, the transition between rebound and coalescence was principally dictated by the normal Weber number, defined as

$$We = \frac{\rho V^2 R}{\sigma}, \tag{1.1}$$

where ρ is the fluid density, V is the droplet impact velocity projected normal to the undisturbed bath interface, R is the droplet radius and σ is the surface tension (figure 1*a*). The BC transition was further interrogated for oblique streams of droplets in numerous follow-up works (Jayaratne & Mason 1964; Ching, Golay & Johnson 1984; Zhbankova & Kolpakov 1990; Doak *et al.* 2016), where various hypotheses about the possible role of relative tangential motion have been proposed, but have hitherto lacked any experimental backing.

Single droplets may also rebound from a quiescent fluid bath, with the BC transition occurring above a critical Weber number that depends on the liquid and gas properties (Rodriguez & Mesler 1985; Pan & Law 2007; Huang & Zhang 2008; Zhao, Brunsvold & Munkejord 2011; Zou *et al.* 2011; Tang *et al.* 2016, 2018; Wu *et al.* 2020; Wu & Saha 2022). Although the depth (H) of the fluid bath also plays a critical role in determining the outcome when it is of the order of the droplet size (Pan & Law 2007), our focus here is on the case of deep baths where $H \gg R$. Despite the considerable progress over the last several decades, these prior works have focused exclusively on the axisymmetric case of normal droplet impacts on a still fluid bath. At this point it remains unknown what role tangential motion might play in determining the transition between bouncing and coalescence, and in particular, if the normal Weber number is sufficient to determine the outcome. Herein, we experimentally demonstrate that relative bath motion leads to a systematic reduction in the critical normal Weber number. This finding is in contrast to other scenarios where relatively rapid substrate translation has been shown to favour non-coalescence behaviour (Neitzel & Dell'Aversana 2002; Che, Deygas & Matar 2015; Castrejón-Pita *et al.* 2016; Gauthier *et al.* 2016; Sprittles 2024), although in some scenarios a small radial boundary flow has been shown to enhance air-layer drainage and accelerate coalescence (Lo, Liu & Xu 2017). Companion three-dimensional direct numerical simulation (DNS) results allow us to interrogate the air-layer dynamics during impact and isolate the mechanism responsible for the reduction.

2. Experimental methods

2.1. *Experimental set-up*

A rendering of the experimental set-up is shown in figure 1(*b*). Droplets of silicone oil are generated from a piezoelectric droplet-on-demand generator (Harris, Liu & Bush

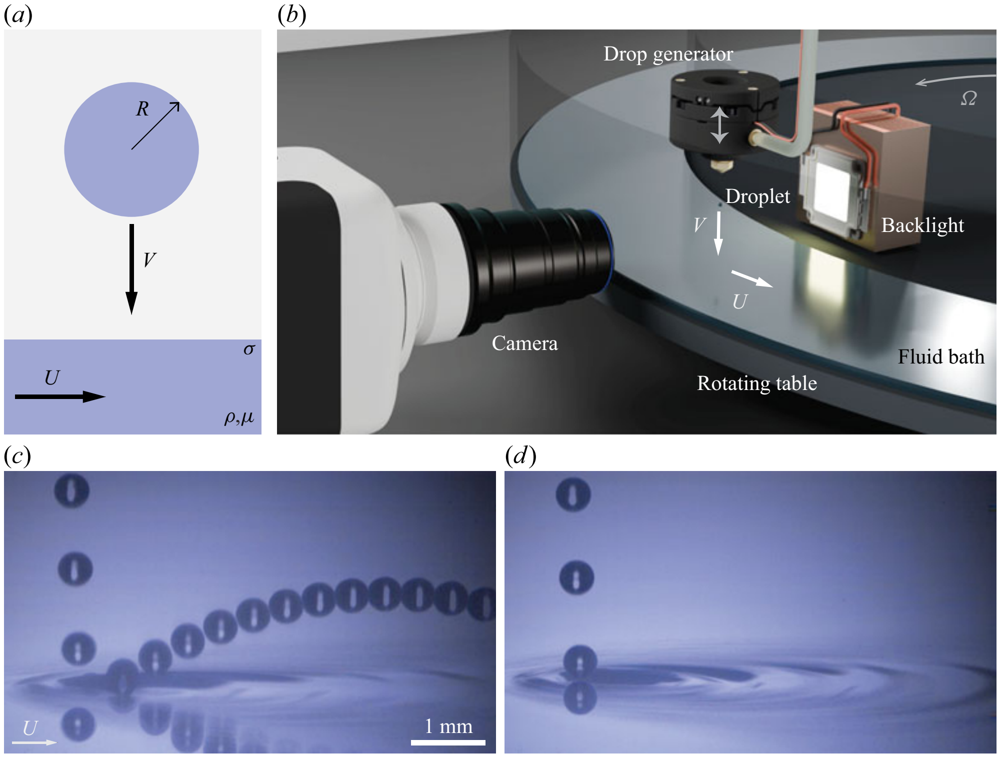

Figure 1. (*a*) Schematic of a droplet impacting a moving bath of the same fluid. (*b*) Rendering of experimental set-up. A droplet is generated by a piezoelectric droplet generator and impacts a moving fluid layer atop a rotating table. The dynamics is filmed from the side with a high-speed video camera. (*c*, *d*) A 2 cSt silicone oil droplet of radius $R = 0.230 \pm 0.006$ mm ($Bo = 0.024$, $Oh = 0.028$) impacts a fluid bath moving with horizontal speed $U = 35$ cm s^{-1}. Images spaced by 1/540 s are directly superimposed. (*c*) With an impact velocity of $V = 59.3 \pm 0.9$ cm s^{-1}, the droplet rebounds from the fluid bath while obtaining a horizontal velocity from the bath during contact. (*d*) At $V = 60.7 \pm 0.8$ cm s^{-1}, the droplet merges with the bath and the residual interfacial disturbance is transported downstream following coalescence. Supplementary movies are available at https://doi.org/10.1017/jfm.2026.11232.

2015; Ionkin & Harris 2018) and impact a fluid bath of the same fluid. The working fluids are silicone oil (Clearco Products) with kinematic viscosities $\nu = \mu/\rho = 2$, 20 and 50 cSt. These fluids correspond (respectively) to densities of $\rho = 0.873$, 0.949 and 0.960 g cm^{-3} and surface tension coefficients of $\sigma = 18.7$, 20.6 and 20.8 dynes cm^{-1}, as provided by the manufacturer datasheet. The latest version of the generator, and the one employed for this work, is documented at https://github.com/harrislab-brown/DropGen. Interchangeable nozzles allow for control of the droplet radius – commercial 3D-printer nozzles of outlet diameter 0.3, 0.5 and 1.0 mm are used in the present work, resulting in droplet sizes in the range $R = 0.17–0.44$ mm. Smaller droplets ($R \approx 0.1$ mm) were successfully produced with a 0.2 mm diameter nozzle, however, the BC transition velocity could not be exceeded with gravity alone (only bouncing observed at their terminal velocity). Apart from very small droplets ($R \lesssim 100$ μm), the BC transition has been documented to be largely insensitive to the droplet radius (Schotland 1960; Pan & Law 2007; Lewin-Jones 2024). The acceleration due to gravity is given by g. The fluid and droplet sizes used correspond to Bond numbers ($Bo = \rho g R^2/\sigma$) ranging from 0.01 to 0.09 and Ohnesorge numbers ($Oh = \mu/\sqrt{\rho\sigma R}$) ranging from 0.02 to 0.5, suggesting that gravity and viscosity play a secondary role, with the dynamics dominated by inertia and capillarity (Alventosa, Cimpeanu & Harris 2023). The droplet generator head is mounted on a vertically oriented motorised translation stage controlled by a stepper motor that allows for vertical displacement of the generator (with resolution of 1280 steps per mm) in order to vary the droplet impact velocity, and therein the Weber number.

Horizontal motion of the liquid bath is achieved via a large rotating table, with design and construction inspired by the 'weather in a tank' apparatus (Illari *et al.* 2009). The rotating circular platform has a diameter of 0.71 m and is driven into steady rotation at speeds up to $\Omega = 10$ rpm by a friction wheel. The fluid is confined within an annulus with inner diameter 0.61 m surrounded on either side by thin clear walls of height 7.6 cm and thickness 4.7 mm. A similar rotating annular bath set-up has been used in prior work to study the rebound of vertical fluid jets impacting a translating fluid bath (Thrasher *et al.* 2007). The annulus is filled with 1 l of silicone oil corresponding to a mean fluid depth of 4.5 mm. Prior work has demonstrated that depths greater than approximately 2–3 droplet radii correspond to deep-bath limit for the BC threshold (Pan & Law 2007; Tang *et al.* 2018; Wu & Saha 2022), the regime of interest for the present work. The droplet generator is positioned such that each droplet impacts at the centre of the annular region. Bath linear translation speeds (as evaluated at the impact location) of up to $U = 35\ \mathrm{cm\ s^{-1}}$ are achieved with the design and explored in the present work. The speed is monitored by an encoder attached to a second spring-loaded friction wheel and held constant via closed-loop feedback control. Maximum uncertainty in the bath speed U at the impact position was estimated to be 2 % of the reported value. Inevitably, the table rotation leads to a curved parabolic interface shape in steady state. At the maximum speed used in the present work, the interface has an estimated 2.2° inward slope at the impact location. The annular bath is covered when not in use to minimise ambient contamination. We note that in the reference frame of the bath, the problem is one of an oblique droplet impact with an incident angle relative to the horizontal of $\tan\theta = V/U$, albeit with a potentially different air boundary layer dynamics.

The dynamics is imaged through the outer annulus with a high-speed video camera (Phantom Miro LC 311) and macro lens (Laowa 25 mm Ultra Macro) at a frame rate of 15 000 frames per second, exposure time of 50 µs and spatial resolution of 7.8 µm per pixel. The droplet and bath are illuminated using a custom LED backlight. To clearly view the droplet and bath interface in all cases the camera is angled downward at 8°, leading to small errors on distances and speeds of no more than 1 %. A transition from BC following a slight increase in V is shown in figures 1(*c*) and 1(*d*).

2.2. *Experimental procedure*

To start an experiment, the bath is set at the desired linear speed and left to equilibrate for several minutes before experiments are performed. Droplets are then generated at a frequency of 2 Hz or slower. The generator is positioned sufficiently high such that all droplets coalesce. The generator is then lowered by 1.0 mm and 15 successive droplet impacts are observed. The lowering process is repeated until at least 13 of 15 of the observed droplets rebound, at which point a single video recording is taken for droplet size and velocity measurements. The generator is then raised by 1.0 mm until 13 of 15 droplets coalesce, and another video is taken. This process (incremental lowering/raising) is repeated twice more before moving to a new table speed. After surveying all table speeds, the overall procedure is repeated twice more for a total of three complete trials. This protocol results in a total of nine measurements of the bouncing threshold and nine measurements of the coalescence threshold at each table speed. The criterion of 13 of 15 was chosen to robustly deal with outliers that occur even away from the transition point, presumably resulting from ambient vibrations, air currents, surface contamination and other inevitable imperfections. The transition between regimes occurs over a relatively narrow range of impact velocities, typically of the order of 2 cm s^{-1}. The video recordings are post-processed in MATLAB using Canny edge detection to obtain the droplet radius and velocities as in prior work (Galeano-Rios *et al.* 2021; Alventosa *et al.* 2023). In the experiment, the contact time t_c is defined as the duration between the frame where the highest point of the droplet is one diameter above the undisturbed free surface (i.e. $z = 2R$) to the frame where it returns to that same height. For computation of the vertical impact velocity, a parabola is fit to at least 25 points prior to impact for the vertical location of the highest point of the droplet, $z(t)$. The slope of the fitted parabola is then evaluated at the impact frame (defined as $t = 0$), yielding the incident vertical (normal) velocity V. A similar protocol is followed for the horizontal velocity, where a line is fit to the horizontal location of the highest point of the droplet $x(t)$, and derivative evaluated at $t = 0$ yielding the incident horizontal velocity U_i. On average, U_i was less than 9 % of the pool speed U, and likely a consequence of the air boundary layer driving some lateral motion prior to impact. The same procedure was followed for the outgoing vertical (V_e) and horizontal (U_e) velocities, fitting a parabola and line to $z(t)$ and $x(t)$, respectively, for at least 70 points after impact, and evaluating the derivatives at $t = t_c$. The vertical coefficient of restitution was then computed as $\alpha = V_e/V$ and the horizontal coefficient of restitution as $\epsilon = \Delta U/U = (U_e - U_i)/U$.

3. Direct numerical simulation

Complementing the experimental set-up deployed in this study, we have developed a three-dimensional numerical counterpart using the open-source software Basilisk (Popinet 2009, 2015), which has been successfully used for studying bouncing phenomena recently (Alventosa *et al.* 2023; Sanjay, Chantelot & Lohse 2023; Ray *et al.* 2024; Phillips, Cimpeanu & Milewski 2025). Our multi-scale framework, balancing the requirement to resolve the thin gas film entrapped between the impacting drop and the moving pool, with a sufficiently large-scale domain to ensure the rebound is unaffected by finite size effects, make it an ideal candidate for the adaptive mesh refinement and parallelisation features of the code. The full implementation is made available at https://github.com/rcsc-group/BouncingDropletsMovingPool3D. The domain construction builds on a computational box measuring 20^3 dimensionless units (relative to a dimensionless impacting drop radius of 1), making use of the one viable symmetry plane (the $x-z$ plane), and is illustrated in figure 2(*a*). This choice ensures that outward-propagating waves have sufficient space to develop and exit the domain cleanly. The droplet is initialised with its south pole one radius above the pool, and a uniform imposed vertical velocity field within. Gravitational effects are also included in the simulation set-up. Inflow boundary conditions (and in particular a non-zero horizontal velocity in x) are employed across one face of the cube, with free slip and impermeability prescribed at the bottom of the geometry, and outflow conditions on all other boundaries. The noted uniform directional horizontal velocity field is prescribed in both pool and gas regions, replicating a fully developed flow near the rotating table liquid–gas surface. The air boundary layer above the rotating fluid surface in the experiment can be estimated using the expression $\delta \approx 2.5(\mu_a L/(\rho_a U))^{1/2}$, where L is the radial position of impact on the table, and μ_a and ρ_a are the viscosity and density of air, respectively (Gauthier *et al.* 2016). Across all speeds, $\delta \gtrsim 6$ cm, which is substantially larger than the computational domain and justifies the use of a uniform air inlet condition. We find that the horizontal velocity induced by the imposed non-zero horizontal air flow during the transient stage prior to impact imparts a change of less than 1 % in the horizontal velocity of the drop

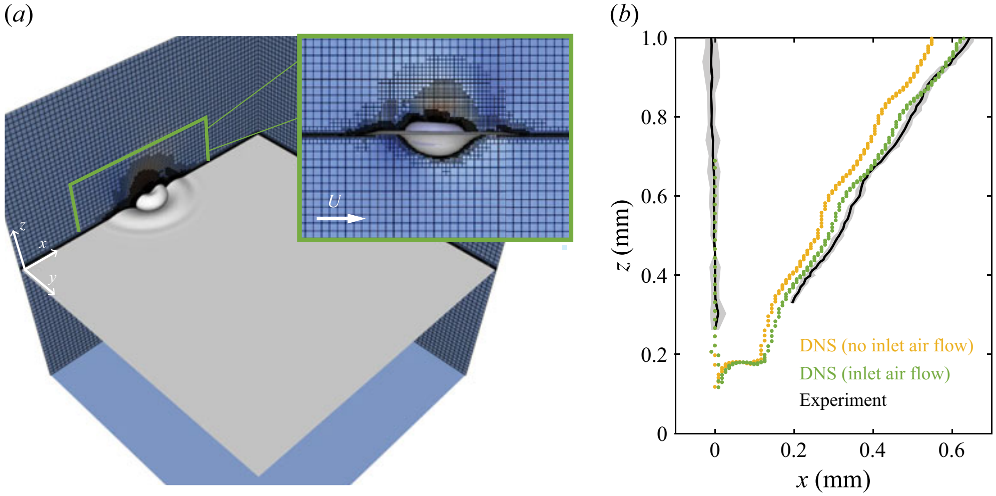

Figure 2. (a) Three-dimensional computational domain for the DNS, with adaptive mesh construction highlighted in the inset. Supplementary movies of representative test cases (impact onto both static and moving pools) are also made available as Supplementary Movies 2 and 3. (b) Trajectory of highest point of droplet in the symmetry plane for a case of a 2 cSt silicone oil droplet with $R = 0.23$ mm ($Bo = 0.024$, $Oh = 0.028$), $V = 60.3\ \mathrm{cm\,s^{-1}}$ and $U = 15\ \mathrm{cm\,s^{-1}}$. Yellow markers are predictions without inlet airflow, green markers are predictions with uniform inlet airflow, and solid lines are experimental measurements. The shaded region represents two standard deviations across experimental trials.

(measured at its centre of mass) relative to the initially imposed vertical velocity. The extremal case in our study, wherein the ratio between the horizontal velocity of the pool and vertical velocity of the drop is approximately 0.5, translates to an increase of 0.371 % in the horizontal velocity component of the drop just prior to impact. Ensuring that the gas region has a non-zero velocity was found nevertheless to be crucial for good agreement with experiments in scenarios in which the horizontal velocity of the pool was non-negligible ($\gtrsim 10\,\%$) relative to the vertical drop velocity, as showcased in figure 2(b). Furthermore, the uniform inflow condition makes our results directly applicable to the case of an oblique droplet impact, as the problem is identical when shifted into the inertial reference frame of the bath.

The set-up described above, equipped with a mesh refinement strategy based on the position of the liquid–gas interfaces, as well as changes in magnitude of velocity components and vorticity, leads to tractable configurations with $O(10^6)$ computational grid cells, which are executed over 20 dimensionless time units (typically equivalent to $O(10^{-2})$ s in dimensional terms). This computation can be achieved in approximately $2000-3000$ CPU hours for each run, executed on local high performance computing clusters over 8–16 CPUs. Following careful verification and previous investigations (Alventosa *et al.* 2023), we found that a minimum cell size measuring $O(1)$ μm (typically 4.49 μm when using 2^{10} grid cells per dimension as the most refined cell size) is sufficient to ensure mesh-independent results in the target metrics. Appendix A includes a detailed mesh resolution study that underpins this conclusion. Classical quantities of interest such as contact time and coefficients of restitution are shown to converge at this level of refinement, while the behaviour of the gas film thickness is sufficiently robust so as to enable reliable interrogation and to support mechanistic explanations. This resolution is also well aligned with previous entrapped gas film measurements in this regime (Tang *et al.* 2019), albeit without three-dimensional flow features. Few comprehensive numerical

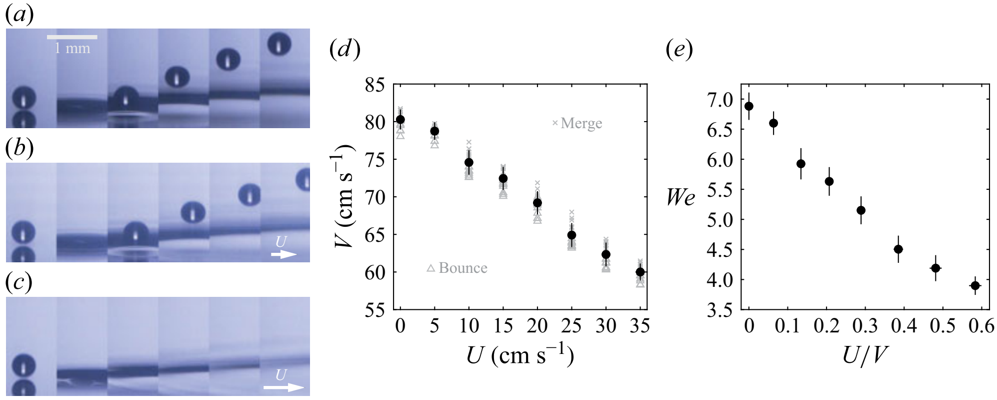

Figure 3. Droplets (2 cSt silicone oil) of radius $R = 0.230 \pm 0.006$ mm ($Bo = 0.024$, $Oh = 0.028$) with incident vertical speed V impact a fluid bath moving with horizontal speed U. (*a–c*) Fixed impact velocity $V = 73.1 \pm 1.0$ cm s^{-1} with increasing bath speed. Successive images in each sequence are spaced 1/750 s apart. Bouncing is observed for (*a*) $U = 0$ cm s^{-1} and (*b*) $U = 10$ cm s^{-1}, with merging at (*c*) $U = 20$ cm s^{-1}. Corresponding videos available in Supplementary Movie 4. (*d*) Bouncing to coalescence transition as a function of bath speed. Grey triangles are trials where bouncing was observed, grey × symbols are trials where coalescence was observed, and black markers are the mean transition values at each bath speed. (*e*) Critical *We* as a function of normalised bath speed U/V. In all cases error bars represent propagated error, including one standard deviation across trials.

studies have been considered in fully three-dimensional domains given the high numerical cost, however, there are excellent examples in both bouncing (Ramírez-Soto *et al.* 2020) and splashing (Wang *et al.* 2023) contexts, with the authors highlighting the considerable resources required to fully resolve the features of interest in the target regimes across a sufficiently wide section of the parameter space.

In our implementation, coalescence between the drop and the pool is prevented at the level of the volume-of-fluid method by construction (similar to the approach in Ramírez-Soto *et al.* (2020)) to avoid artificial merging that could disrupt the bouncing dynamics. With careful mesh adaptivity, this approach yields mesh-independent results but cannot naturally capture coalescence, which would require sub-continuum physics considerations (Lewin-Jones, Lockerby & Sprittles 2024). Instead, we use our numerical infrastructure to probe bouncing regimes identified experimentally, providing mechanistic insight and enabling detailed analysis of rebound dynamics and air-layer evolution in this delicate regime.

4. Results

Consistent with what is known from prior work on axisymmetric impacts (and showcased in figure 1(*c*) and 1(*d*)), for a given set of parameters, there is a critical vertical impact velocity V at which the behaviour transitions from bouncing to merging. The goal of the present work is to explore how the introduction of translational bath speed U influences this critical velocity. An experimental sequence is shown in figure 3, where now the vertical velocity is fixed, and the bath speed is increased incrementally. At $U = 0$ cm s^{-1}, the droplet rebounds in an axisymmetric manner, as expected. For $U = 10$ cm s^{-1}, the droplet also successfully rebounds, but departs the surface with a non-zero horizontal velocity bestowed onto it by the bath. However, as the speed is increased further to $U = 20$ cm s^{-1}, merging ensues, suggesting that the bath motion has introduced new conditions favourable to air-layer drainage. For fixed droplet size and fluid parameters,

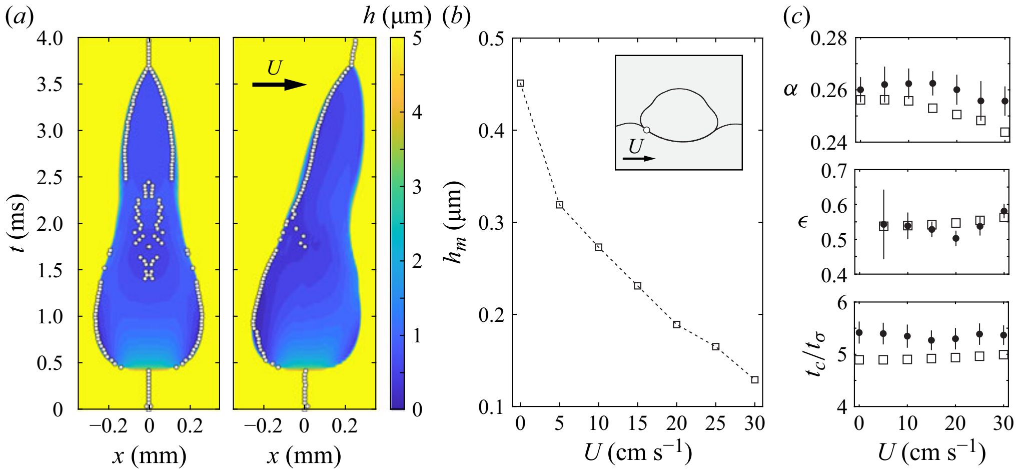

Figure 4. Simulation results of droplets (2 cSt silicone oil) of radius $R = 0.23$ mm ($Bo = 0.024$, $Oh = 0.028$) with incident vertical speed $V = 60.3$ cm s^{-1} impacting a fluid bath moving with horizontal speed U. (*a*) Evolution of air-layer thickness profile along symmetry plane for the case of $U = 0$ (left) and $U = 15$ cm s^{-1} (right). Circular markers indicate the point of minimum thickness, which systematically occurs on the upstream side of the contact region for $U > 0$. (*b*) Minimum air-layer thickness as a function of bath speed U. Inset shows a typical slice from the simulation, with the circular marker indicating the position of minimum thickness. (*c*) Vertical coefficient of restitution (α), horizontal coefficient of restitution (ϵ), and non-dimensional contact time (t_c/t_σ) as a function of U for simulations (□) and experiments (●). Here, t_σ is the inertio-capillary time scale defined as $\sqrt{\rho R^3/\sigma}$. For experimental data, error bars represent propagated error, including one standard deviation across trials.

this effect is explored systematically in figure 3(*d*). Individual trials for the bouncing and merging threshold are shown as the grey markers, with the combined data summarised by the black markers. As can clearly be seen, the bath motion U leads to a systematic reduction in the necessary vertical velocity required to initiate merging. The non-dimensionalised version is presented in figure 3(*e*), again highlighting this monotonic trend.

As reviewed in the introduction, the persistence of the intervening air layer determines the impact outcome. As such, our experimental observations suggest that the evacuation of the air layer is enhanced by the motion of the bath. To elucidate the physical mechanism underlying this conclusion, we turn to our companion numerical simulations. In figure 4(*a*), the thickness of the air layer in the symmetry plane is plotted as it evolves in time for a representative bouncing case with and without bath motion. For the case of $U = 0$, the air layer evolves symmetrically, as expected, with the minimum air gap thickness (denoted by the circular markers) occurring on the rim of the contact region for most of the contact period. The draining of the air gap exhibits a rich dynamics even in this base scenario, with the draining of the gas film and the transition from ascent to descent stages leading to jumps in the location of the minimum from the rim towards the south pole of the drop and back, as illustrated during a time scale approximately described by $1.5 < t < 2.5$ ms in the leftmost panel. This delicate interplay has been reported previously in the normal impact scenario by Tang *et al.* (2019), withstanding significant parametric variation. Introducing bath motion breaks this symmetry, and in particular, the location of minimum thickness now systematically occurs on the upstream edge of the contact region, with a much shorter-lived switching period around $t \approx 1.8$ ms in which the minimum is found closer to the south pole of the drop. Figure 4(*b*) shows the absolute minimum thickness as a function of bath speed, demonstrating that the introduction of bath speed also decreases the minimum thickness, consistent with our conclusion that the horizontal motion must enhance air-layer drainage locally, favouring merging behaviour. We note that the reported minimum air gap thickness occurs at a sub-grid cell length scale, thereby requiring a robust post-processing algorithm to ensure that the extracted value is free from numerical interfacial reconstruction errors, is maintained for a sufficiently long time scale to be reliable, and is standardised across different test cases. An imposed criterion of the air-layer thickness being extracted using a rolling window characterised by a length scale of at least 5 adjacent contact grid cells and sustained over 10 % of the contact time was found to provide a suitable balance between avoiding numerically induced artefacts in both space and time, and capturing the defining features of the different stages of the rich bouncing dynamics. Figure 6(*b*) in Appendix A provides an illustration of the gas film dynamics focusing on the contact time scale. We argue that the measurements showcase consistent behaviour and a strong level of robustness across different mesh resolution levels while acknowledging the well-known mesh-dependent properties of the calculation, which makes quantitative predictions unreliable. We therefore aim to use these results in order to understand the impact dynamics and key trends in the obtained measurements. With these considerations and while only drawing from the qualitative trends of the data therein, as depicted in the inset of figure 4(*b*), we find that the depression created by the droplet during impact is pressed against the tilted upstream side of the droplet as the bath continues to translate, and is the mechanism responsible for the enhanced drainage. Although not a primary objective of the article, we also present typical bouncing metrics (coefficients of restitution and contact time) for these parameters in figure 4(*c*), demonstrating that these factors are largely unaffected by the bath motion. Zhbankova & Kolpakov (1990) suggested, but did not demonstrate, that relative tangential velocity might prolong the contact time and ultimately promote air-layer drainage. Here we show that the contact time is essentially constant with U, and therefore a different mechanism is at play behind the favoured coalescence in our experiments.

Lastly, we explore the generality of our main finding: that the normal Weber number for the BC transition decreases with relative bath motion. Figure 5(*a*) presents the results for the critical impact Weber number as a function of normalised bath speed for multiple droplet sizes and viscosities (up to 50 cSt), with the droplet and bath always being of the same fluid. Consistent with prior understanding in the axisymmetric case (Schotland 1960; Pan & Law 2007), the threshold is only weakly sensitive to the droplet size in this regime. We also observe a clear increase in the threshold with increased viscosity, similarly documented and rationalised in prior work on the axisymmetric problem (Tang *et al.* 2018). Nevertheless, in every parameter combination explored herein, the critical We systematically decreases with bath speed. If we replot the data for the critical vertical velocity V, normalised by the axisymmetric critical velocity V_0 (for $U = 0$) in each case, all of the collected data nearly collapse along a single curve in figure 5(*b*). Note that the ratio V/V_0 can also be expressed as $(We/We_0)^{1/2}$, where We_0 is the critical normal Weber number for the equivalent axisymmetric case. This collapse, which involves only kinematic parameters of the problem, suggests a geometric interpretation of our result. As discerned from the simulation, the tilted upstream contact surface and the relative bath motion conspire to promote upstream air-layer drainage. If one then assumes air-layer evacuation is caused by the normal projection of both V and U onto a tilted surface with angle ϕ (see inset of figure 5(*b*)), a new characteristic velocity for the transition can be defined as $V_c = V\cos\phi + U\sin\phi$. When $U = 0$, $V_c = V_0\cos\phi$, and we can find

$$\frac{V}{V_0} = \frac{1}{1 + \dfrac{U}{V}\tan\phi}. \tag{4.1}$$

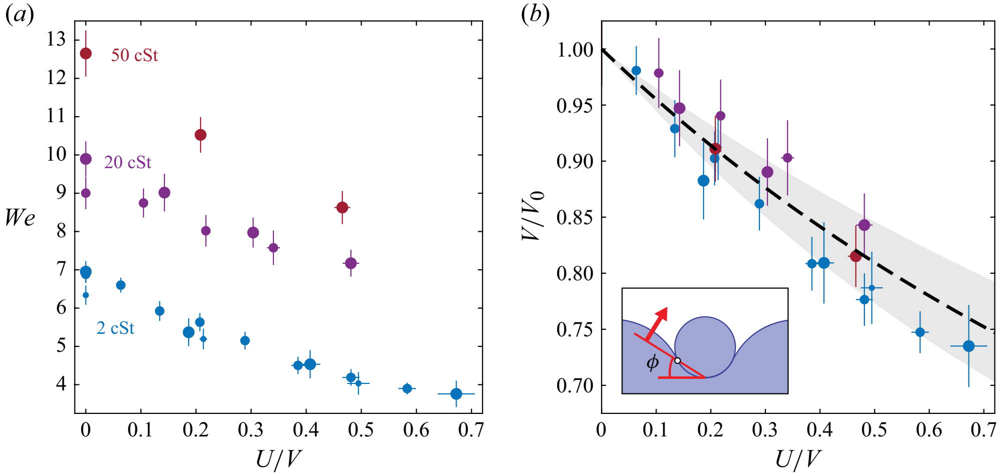

Figure 5. (*a*) Bouncing to coalescence transition for silicone oil droplets of different viscosities (marker colour) and radii (marker size) as a function of the normalised bath speed. For 2 cSt oil (blue): small, medium and large markers correspond to $R = 0.169 \pm 0.008$, 0.230 ± 0.006 and, 0.403 ± 0.008 mm, respectively ($Bo = 0.013$, 0.024, 0.074 and $Oh = 0.033$, 0.028, 0.022). For 20 cSt oil (purple): medium and large markers correspond to $R = 0.208 \pm 0.009$ and 0.398 ± 0.008 mm, respectively ($Bo = 0.020$, 0.071 and $Oh = 0.30$, 0.22). For 50 cSt oil (red): large markers correspond to $R = 0.443 \pm 0.016$ mm ($Bo = 0.089$ and $Oh = 0.51$). In all cases, droplets impact onto a bath of identical fluid. (*b*) Critical vertical velocity V normalised by the critical velocity for a still bath V_0 (i.e. with $U = 0$) under otherwise equivalent conditions. The dashed line (and shaded region) shows expression (4.1) with film angle parameter $\phi = 25.2 \pm 5.2^\circ$. The ratio V/V_0 can also be expressed as $(We/We_0)^{1/2}$, where We_0 is the critical normal Weber number for the equivalent axisymmetric case. In all cases error bars represent propagated error, including one standard deviation across trials.

Fitting the best value of ϕ to each dataset yields $\phi = 25.2 \pm 5.2^\circ$, which is consistent with the typical average film slopes observed in our simulations and those of Lewin-Jones (2024) for the axisymmetric scenario. While the details of the gas film evolution are dynamic and complex, our combined results nevertheless suggest a simple coherent physical picture. The deformation of the bath caused by the droplet impact itself leads to a tilted mediating air film, with drainage on the upstream side then enhanced by the relative bath motion. Crudely approximating the substrate as a tilted planar surface with angle $\phi \approx 25^\circ$ allows us to rationalise the collapse of all our data, motivated by this simple geometric understanding of the underlying physical mechanism at play. The successful collapse of the transition data with this geometric viewpoint suggests a revised definition of the critical Weber, $We_c = \rho(V \cos\phi + U \sin\phi)^2 R/\sigma$, that generalises beyond the axisymmetric scenario.

5. Discussion

Despite the progress presented herein, there are some limitations that should be noted and may also serve as motivation for future work. Due to experimental constraints, the study was restricted to scenarios where $U < V$ (corresponding to near-normal impacts in the equivalent oblique problem). It is plausible that higher bath speeds (or shallow impact angles as in Leneweit *et al.* (2005)) would result in different phenomenology. In particular, aerodynamic levitation of droplets has been documented in cases with higher substrate speeds ($U \gtrsim 1$ m s^{-1}) (Castrejón-Pita *et al.* 2016; Gauthier *et al.* 2016), which suggests the possibility of a non-monotonic trend in the critical Weber number. Furthermore, the present work focuses on millimetric droplets, whereas it has been shown that for the case of both oblique droplet streams and single droplets impacting normally, small droplets ($R \lesssim 100\,\mu\mathrm{m}$) exhibit an additional coalescence regime that precedes the bouncing regime (Jayaratne & Mason 1964; Bach, Koch & Gopinath 2004; Zhao *et al.* 2011; Lewin-Jones 2024), leading to a coalescence–bouncing–coalescence transition sequence as the Weber number is increased from zero. Future work on the topic might also explore the role of layer depth (Pan & Law 2007), charge (Jayaratne & Mason 1964), differing drop and bath fluids (Wu & Saha 2022), ambient gas properties (Schotland 1960), wind (Liu 2018), curved interfaces (such as sessile droplets (Moon *et al.* 2018)) or unsteady fluid interfaces (Couder *et al.* 2005; Che *et al.* 2015). In particular, future experiments with differing bath and droplet viscosities would be particularly valuable towards further elucidating the subtle role of substrate deformation in defining the BC transition. From the modelling perspective, additional work extending the hybrid open-source computational framework of Sprittles (2024) and Lewin-Jones (2024) to three dimensions would provide additional physical insight and a predictive capability currently unavailable for this highly multi-scale problem.

Supplementary movies. Supplementary movies are available at https://doi.org/10.1017/jfm.2026.11232.

Funding. The authors gratefully acknowledge the financial support of the National Science Foundation (NSF CBET-2123371) and the Engineering and Physical Sciences Research Council (EPSRC EP/W016036/1).

Declaration of interests. The authors report no conflicts of interest.

Data availability statement. The DNS implementation, as well as associated data pre- and post-processing scripts are made available at https://github.com/rcsc-group/BouncingDropletsMovingPool3D. Data are available from the corresponding author upon request.

Appendix A. Numerical resolution study

The numerical study in this investigation represents a non-trivial and computationally resource-intensive campaign that greatly benefits from the capabilities of the underlying algorithmic set-up in Basilisk. In § 3 we have introduced key structural elements of our implementation. In what follows we expand on performance and result robustness aspects, with the reference test case previously illustrated in figure 2 and the surrounding discussions as its basis. This case represents an impact scenario onto a pool moving at a moderate speed (half-way through the parameter sweep in our study for the variable in question), readily leading to the (symmetry-breaking) behaviour of interest in the three-dimensional flow.

In order to ascertain the appropriate resolution level for the results in this work, we have focused on balancing accuracy and efficiency, considering several target quantities that encapsulate a full range of detail from highly temporally and spatially localised features such as the gas film thickness to larger-scale metrics such as contact time and coefficients of restitution, thereby providing a stringent test for our platform. We summarise our findings in figure 6 and table 1, respectively.

The typical vertical dynamics during impact is shown in figure 6(*a*), with the top of the drop, its centre of mass and its bottom coordinates being overlaid with the height of the liquid pool just underneath the drop. While our lowest resolution level 8 (representing 2^8 grid cells per dimension for our domain spanning 20 drop radii in each dimension) has small deviations compared with its more refined counterparts (as highlighted in the magnified inset), we overall find excellent alignment across resolution levels for the droplet dynamics, translating into suitably converged values for traditional bounce metrics such as contact time and coefficients of restitution. The horizontal dynamics

Resolution level	CPU runtime (s)	Grid cell count	Min. grid cell size (μm)	Min. gas film thickness (μm)	Vertical CoR (α)	Horizontal CoR (ϵ)	Contact time t_c/t_σ
8	1.90×10^4	$1.0-1.5\times10^5$	17.969	1.127	0.254	0.517	4.848
9	1.85×10^5	$4.2-5.6\times10^5$	8.984	0.473	0.251	0.538	4.919
10	3.46×10^6	$1.8-1.9\times10^6$	4.492	0.231	0.252	0.541	4.917
11	3.12×10^7	$8.0-8.5\times10^6$	2.246	0.188	0.253	0.542	4.915

Table 1. DNS resolution study for the impact and subsequent bounce of a 2 cSt silicone oil droplet with $R = 0.23$ mm ($Bo = 0.024$, $Oh = 0.028$), $V = 60.3$ cm s^{-1} and $U = 15$ cm s^{-1}, as the prototypical test case in our study. Here, we highlight performance metrics (CPU runtime, grid cell count), geometrical information (minimum grid cell size) and the convergence properties of metrics of interest such as the horizontal (ϵ) and vertical (α) coefficients of restitution, the normalised contact time and the minimum gas film thickness.

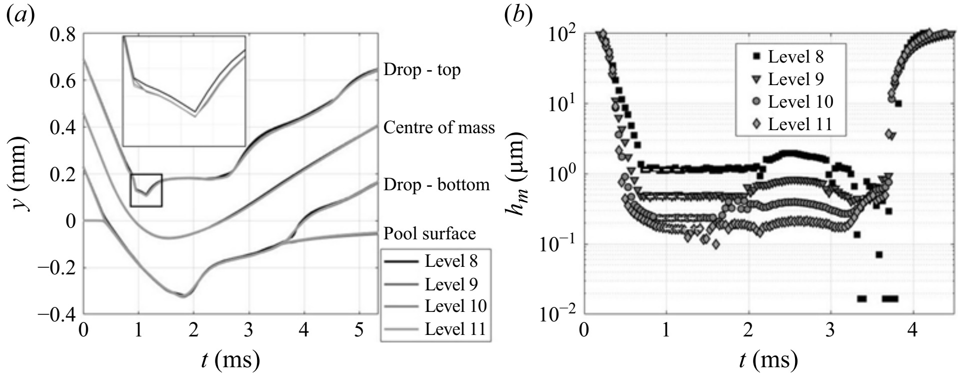

Figure 6. Resolution study for the case of a 2 cSt silicone oil droplet with $R = 0.23$ mm, $V = 60.3$ cm s^{-1} and $U = 15$ cm s^{-1}, as previously presented in figure 2. Four resolution levels, with minimum grid cell sizes ranging from 17.969 μm (level 8) down to 2.246 μm (level 11), and further properties detailed in table 1, are considered. (*a*) Interfacial dynamics of drop vertical coordinate y extracted at the plane of symmetry with the droplet minimum and maximum coordinates, as well as its centre of mass, illustrated alongside the measured pool deformation during the impact evolution. The inset zooms in onto a time scale of large deformation for the top of the drop, when small differences are most visible. (*b*) Minimum gas film thickness across the contact region at regular discrete points in time during the bouncing dynamics. The while horizontal dashed lines (found at $t \approx 1$ ms for each case) show the values which are extracted as describing the minimum film thickness reported in each case.

(z versus t) showcases very similar behaviour upon inspection. This comparison gives us confidence to explore the contact dynamics more carefully towards uncovering explanatory mechanisms and trends that connect to the experimental findings. Figure 6(*b*) displays the minimum thickness obtained across the contact surface, with a sharp decrease as the drop approaches the pool, followed by a plateau-like behaviour as the drop is in its descent phase, during which the reported minimum is extracted (shown as white dashed lines in the respective figure). Comparing the two panels allows us to observe the descent and ascent stages, respectively, including occasionally noisy measurements, particularly at lower resolutions. This noise has encouraged us to formulate the post-processing algorithm mentioned in the discussion of figure 4(*b*), based on ensuring the reported minimum thickness is maintained over sufficiently long spatial and especially temporal scales. Through numerical experimentation it was found that building a criterion based on the average over a rolling window spanning 5 adjacent contact grid cells leading to a measured film thickness maintained over 10 % of the contact time yielded informative results with limited impact from localised numerical artefacts. Across our studies, it is within the descent period (when the drop presses onto the pool surface and the horizontally moving pool also acts to thin out the gas layer) that the overall minimum is found at all resolution levels. There is, however, a rich nonlinear dynamics exhibited throughout the contact period as the competing mechanisms shift during impact and rebound.

In light of the above, we conclude that an $O(\mu\text{m})$-sized minimum grid cell set-up enables us to reconcile our approach with our objectives, with resolution level 10 deemed to be a suitable compromise between robustness and computational cost across our numerical campaign. While careful to differentiate between quantitative predictive capabilities (e.g. for the bounce metrics) and qualitative insight (e.g. for the gas film thickness behaviour), we propagate this set-up to our parameter studies in § 4, while also setting it as a template for the GitHub code repository associated with our investigation.

REFERENCES

ALVENTOSA, L.F.L., CIMPEANU, R. & HARRIS, D.M. 2023 Inertio-capillary rebound of a droplet impacting a fluid bath. *J. Fluid Mech.* **958**, A24.

BACH, G.A., KOCH, D.L. & GOPINATH, A. 2004 Coalescence and bouncing of small aerosol droplets. *J. Fluid Mech.* **518**, 157–185.

CASTREJÓN-PITA, J.R., MUÑOZ-SÁNCHEZ, B.N., HUTCHINGS, I.M. & CASTREJÓN-PITA, A.A. 2016 Droplet impact onto moving liquids. *J. Fluid Mech.* **809**, 716–725.

CHE, Z., DEYGAS, A. & MATAR, O.K. 2015 Impact of droplets on inclined flowing liquid films. *Phys. Rev. E* **92** (2), 023032.

CHING, B., GOLAY, M.W. & JOHNSON, T.J. 1984 Droplet impacts upon liquid surfaces. *Science* **226** (4674), 535–537.

COUDER, Y., FORT, E., GAUTIER, C.-H. & BOUDAOUD, A. 2005 From bouncing to floating: noncoalescence of drops on a fluid bath. *Phys. Rev. Lett.* **94** (17), 177801.

DOAK, W.J., LAIACONA, D.M., GERMAN, G.K. & CHIAROT, P.R. 2016 Rebound of continuous droplet streams from an immiscible liquid pool. *Phys. Fluids* **28** (5), 057104.

GALEANO-RIOS, C.A., CIMPEANU, R., BAUMAN, I.A., MACEWEN, A., MILEWSKI, P.A. & HARRIS, D.M. 2021 Capillary-scale solid rebounds: experiments, modelling and simulations. *J. Fluid Mech.* **912**, A17.

GAUTHIER, A., BIRD, J.C., CLANET, C. & QUÉRÉ, D. 2016 Aerodynamic Leidenfrost effect. *Phys. Rev. Fluids* **1** (8), 084002.

HARRIS, D.M., LIU, T. & BUSH, J.W.M. 2015 A low-cost, precise piezoelectric droplet-on-demand generator. *Exp. Fluids* **56**, 1–7.

HUANG, Q. & ZHANG, H. 2008 A study of different fluid droplets impacting on a liquid film. *Pet. Sci.* **5** (1), 62–66.

ILLARI, L., *et al.* 2009 Weather in a tank. *B. Am. Meteorol. Soc.* **90** (11), 1619–1632.

IONKIN, N. & HARRIS, D.M. 2018 Note: a versatile 3D-printed droplet-on-demand generator. *Rev. Sci. Instrum.* **89** (11), 116103.

JAYARATNE, O.W. & MASON, B.J. 1964 The coalescence and bouncing of water drops at an air/water interface. *Proc. R. Soc. Lond. A* **280** (1383), 545–565.

LENEWEIT, G., KOEHLER, R., ROESNER, K.G. & SCHÄFER, G. 2005 Regimes of drop morphology in oblique impact on deep fluids. *J. Fluid Mech.* **543**, 303–331.

LEWIN-JONES, P. 2024 Liquid drop impacts: when trapped gas nanofilms lead to bouncing. PhD thesis, University of Warwick.

LEWIN-JONES, P., LOCKERBY, D.A. & SPRITTLES, J.E. 2024 Collision of liquid drops: bounce or merge? *J. Fluid Mech.* **995**, A1.

LIU, X. 2018 Experimental study of drop impact on deep-water surface in the presence of wind. *J. Phys. Oceanogr.* **48** (2), 329–341.

LO, H.Y., LIU, Y. & XU, L. 2017 Mechanism of contact between a droplet and an atomically smooth substrate. *Phys. Rev. X* **7** (2), 021036.

MOON, J.H., CHOI, C.K., ALLEN, J.S. & LEE, S.H. 2018 Observation of a mixed regime for an impinging droplet on a sessile droplet. *Int. J. Heat Mass Transfer* **127**, 130–135.

NEITZEL, G.P. & DELL'AVERSANA, P. 2002 Noncoalescence and nonwetting behavior of liquids. *Annu. Rev. Fluid Mech.* **34** (1), 267–289.

PAN, K.-L. & LAW, C.K. 2007 Dynamics of droplet–film collision. *J. Fluid Mech.* **587**, 1–22.

PHILLIPS, K.A., CIMPEANU, R. & MILEWSKI, P.A. 2025 Modelling two-dimensional droplet rebound off deep fluid baths. *Proc. R. Soc. A* **481** (2317), 20240956.

POPINET, S. 2009 An accurate adaptive solver for surface-tension-driven interfacial flows. *J. Comput. Phys.* **228** (16), 5838–5866.

POPINET, S. 2015 A quadtree-adaptive multigrid solver for the Serre–Green–Naghdi equations. *J. Comput. Phys.* **302**, 336–358.

RAMÍREZ-SOTO, O., SANJAY, V., LOHSE, D., PHAM, J.T. & VOLLMER, D. 2020 Lifting a sessile oil drop from a superamphiphobic surface with an impacting one. *Sci. Adv.* **6** (34), eaba4330.

RAY, S., HAN, Y., YUE, Z., GUO, H., CHAO, C.Y.H. & CHENG, S. 2024 New insights into head-on bouncing of unequal-size droplets on a wetting surface. *J. Fluid Mech.* **983**, A25.

Rayleigh 1899 Xxxvi. Investigations in capillarity. *Lond. Edinb. Dublin Phil. Mag. J. Sci.* **48** (293), 321–337.

REIN, M. 1993 Phenomena of liquid drop impact on solid and liquid surfaces. *Fluid Dyn. Res.* **12** (2), 61–93.

RODRIGUEZ, F. & MESLER, R. 1985 Some drops don't splash. *J. Colloid Interface Sci.* **106** (2), 347–352.

SANJAY, V., CHANTELOT, P. & LOHSE, D. 2023 When does an impacting drop stop bouncing? *J. Fluid Mech.* **958**, A26.

SCHOTLAND, R.M. 1960 Experimental results relating to the coalescence of water drops with water surfaces. *Discuss. Faraday Soc.* **30**, 72–77.

SPRITTLES, J.E. 2024 Gas microfilms in droplet dynamics: When do drops bounce? *Annu. Rev. Fluid Mech.* **56** (1), 91–118.

TANG, X., SAHA, A., LAW, C.K. & SUN, C. 2016 Nonmonotonic response of drop impacting on liquid film: mechanism and scaling. *Soft Matt.* **12** (20), 4521–4529.

TANG, X., SAHA, A., LAW, C.K. & SUN, C. 2018 Bouncing-to-merging transition in drop impact on liquid film: role of liquid viscosity. *Langmuir* **34** (8), 2654–2662.

TANG, X., SAHA, A., LAW, C.K. & SUN, C. 2019 Bouncing drop on liquid film: dynamics of interfacial gas layer. *Phys. Fluids* **31** (1), 013304.

THRASHER, M., JUNG, S., PANG, Y.K., CHUU, C.-P. & SWINNEY, H.L. 2007 Bouncing jet: a Newtonian liquid rebounding off a free surface. *Phys. Rev. E* **76** (5), 056319.

WANG, H., LIU, S., BAYEUL-LAINÉ, A.-C., MURPHY, D., KATZ, J. & COUTIER-DELGOSHA, O. 2023 Analysis of high-speed drop impact onto deep liquid pool. *J. Fluid Mech.* **972**, A31.

WU, Z., HAO, J., LU, J., XU, L., HU, G. & FLORYAN, J.M. 2020 Small droplet bouncing on a deep pool. *Phys. Fluids* **32** (1), 012107.

WU, X. & SAHA, A. 2022 Droplet impact on liquid films: bouncing-to-merging transitions for two-liquid systems. *Phys. Fluids* **34** (10), 103313.

YARIN, A.L. 2006 Drop impact dynamics: splashing, spreading, receding, bouncing. *Annu. Rev. Fluid Mech.* **38** (1), 159–192.

ZHAO, H., BRUNSVOLD, A. & MUNKEJORD, S.T. 2011 Transition between coalescence and bouncing of droplets on a deep liquid pool. *Int. J. Multiphase Flow* **37** (9), 1109–1119.

ZHBANKOVA, S.L. & KOLPAKOV, A.V. 1990 Collision of water drops with a plane water surface. *Fluid Dyn.* **25** (3), 470–473.

ZOU, J., WANG, P.F., ZHANG, T.R., FU, X. & RUAN, X. 2011 Experimental study of a drop bouncing on a liquid surface. *Phys. Fluids* **23** (4), 044101.